The effects of cloud-aerosol-interaction complexity on simulations of presummer rainfall over southern China

Kalli Furtado[1], Paul Field[1], Yali Luo[2], Tianjun Zhou[3], and Adrian Hill[1]

[1]Met Office, Exeter, UK
[2]Chinese Academy of Meteorological Sciences, Beijing, China
[3]Institute of Atmospheric Physics, Beijing, China

Correspondence: kalli.furtado@metoffice.gov.uk

Abstract. Convection-permitting simulations are used to understand the effects of cloud-aerosol interactions on a case of heavy rainfall over south China. The simulations are evaluated using radar observations from the South China Monsoon Rainfall Experiment and remotely sensed estimates of precipitation, clouds and radiation. We focus on the effects of complexity in cloud-aerosol interactions, especially processing and transport of dissolved material inside clouds. In particular, simulations with aerosol concentrations held constant are compared with a fully coupled cloud-aerosol-interacting system to isolate the effects of processing on a line of organised-deep convection. It is shown that in-cloud processing of aerosols can change the vertical structure of squall lines thereby inducing changes in the statistics of surface rainfall. These effects are shown to be consistent with a modulation by aerosol of the timescale of the converting cloud-droplets to rain.

1 Introduction

Physical models of clouds and aerosol microphysics are complex components of atmospheric simulators and, because they are fundamental to the Earth's energy and hydrological cycles, they are a large source of uncertainty in predictions across a wide range of time-scales: from weather forecasts and seasonal predictions, out to climate projections.

Complexity in microphysics schemes arises from the number of processes being modelled and how many prognostic variables are used. Simple single-moment schemes use hydrometeor mass as the prognostic variable for each of cloud droplets, rain and ice. More complex schemes differentiate between sub-species of hydrometeor (graupel, hail, cloud ice and snow) or employ more than one prognostic for each species. Greater complexity improves physical realism but raises the computational expense and it is not obvious where the balance between cost and benefit lies. Moreover, the relative importance of the different mechanisms by which aerosols affect clouds and precipitation are themselves uncertain (Tao , 2012). Although the

basic hypotheses that cloud-droplet number concentrations can alter the brightness, longevities and amounts of clouds are well-established (Twomey , 1977; Albrecht , 1989; Rosenfeld et al , 2008), how these processes combine to determine the responses of systems of clouds has been found to depend on both the system under consideration (Kaufman et al , 2005; Rosenfeld et al , 2008) and the model being used (Hill et al , 2015; Johnson , 2015). For deep-convective clouds in particular, uncertainty

5　abounds because increased droplet numbers are associated with both increased and decreased rainfall in manner that appears sensitive to several factors including: ice formation, the large-scale environment and history of the evolving aerosol-cloud system (Khain et al , 2008; Miltenberger et al , 2018).

A range of complexities are also involved in aerosol schemes. Speciated models treat the population of aerosols as composed of physically distinct species, for example salts of sulphuric acid or sodium, organic- and inorganic-carbon compounds. Each

10　species is distributed across a set of size ranges (modes), the contents of which are described by prognostic variables. Such descriptions clearly necessitate a large number of prognostics.

Cloud-aerosol interactions add further complexity because the sophistication with which these are modelled can itself be varied. In their simplest form, the effect of aerosols on the number concentration, N_c, of droplets or ice crystals, involves parametrizing N_c as a function of the number concentration, N_a, of the aerosol particles:

15　$$N_c = N_{\mathrm{act}}^c(N_a, \dots), \tag{1}$$

where the *ellipsis* $(\dots)$ represents dependencies on other parameters such as atmospheric-state variables. A formulation such as Eq. 1 is suitable for use in a single-moment microphysics scheme, and the aerosol concentration can be a diagnostic parameter or can evolve dynamically via an aerosol scheme.

In microphysics schemes with prognostic cloud-number concentrations, Eq. 1 is modified to take the form of a source term in

20　the dynamical equation for N_c which specifies an increment to the number of cloud particles when the conditions for activation are met.

An advantage of double-moment schemes is that microphysical processes can feedback on aerosol concentration. With a single-moment scheme, the only permitted feedbacks are *sink* terms: aerosols can be depleted during activation but there is no number-conserving way of accounting for in-cloud processing of aerosol material and hence no way of determining how

25　many aerosols are returned to the air when clouds evaporate. Double-moment schemes, because they include a budget for cloud-number concentrations, allow for two-way coupling between aerosols and clouds. In this case, mechanical processing of aerosol inside cloud particles can be modelled explicitly, so particles which acted as cloud nuclei can agglomerate in solution and be re-deposited into the air as larger particles.

The above considerations suggest two levels of aerosol-cloud complexity:

30　　1. *One-way coupling of a fixed population of soluble aerosols.* A parameterization is used for activation of cloud droplets from a fixed population of water-soluble aerosols, but aerosol-number concentrations remain constant[1]. The sole route to nucleation of ice-crystals is via aerosol-independent freezing of cloud droplets.

---

[1]To prevent over-production of cloud-droplets, activation does not occur if the parametrization diagnoses fewer activated droplets than already exist in a grid box. When activation does occur it increases the droplet number to the diagnosed number of condensation nuclei.

2. *Two-way coupled clouds and soluble aerosols.* Aerosols are depleted during activation and aerosol mass is carried through clouds by sedimentation of hydrometeors. and undergoes mechanical processing during collision-coalescence. When hydrometeors evaporate, the air is re-populated with processed aerosols. Because effective cloud nuclei are by definition highly deliquescent, the number concentration of aerosol residuals will equal the number of evaporated hydrometeors. Hence the residuals will typically be less numerous but larger in size than the initial aerosols. In the simplest case, ice nucleation remains independent of aerosols (although, in principle, it could be dealt with in an analogous way).

Two-way coupled schemes were initially developed using detailed size-resolved descriptions of aerosols and clouds (Feingold and Kreidenweis , 2002). However, a more minimal requirement is prognostic variables for the mass and number concentrations of interstitial aerosols and the mass of aerosol present inside each hydrometeor species. (In general, surface emissions of particulates are also required but here we assume that the time-scales for such processes are slow compared to the forecast duration.) Such schemes have recently been incorporated into bulk models of cloud microphysics, but their testing for applications in weather and climate models is still in its relative infancy. In this regard, the study by Miltenberger et al (2018) is of particular relevance to this paper, because it employs the same modeling system. Those authors used the Cloud-AeroSol Interacting Microphysics (CASIM) in regional simulations with the Met Office Unified Model (UM) to investigate the effects of aerosol-cloud interactions on convective clouds over the south-west peninsula of the United Kingdom. They showed that increasing the number of aerosol particles increased the number of convective cells but decreased the mean-cell size. They found that higher concentrations of aerosols suppressed rainfall when the convection was relatively disorganised, but enhanced rainfall when the convection was organised along low-level shear lines (a phenomena that they attributed historical effects of antecedent rainfall on the available moisture as the clouds evolved). In addition, they found that when aerosol processing was included, a simulation with a given initial aerosol concentration tended to behave analogously to a non-processing scheme with a *lower* aerosol concentration (see in particular their Figures 5 and 6).

Fan et al (2012) also examined the effects of *fixed-verses-processed* aerosol concentrations on deep-convective clouds over eastern China. They showed that with both fixed and dynamic aerosols, more polluted conditions were associated with decreased rain water content and suppressed (temporally delayed) rainfall. Their results showed that fixed aerosols exaggerated the responses of cloud and rain to aerosol perturbations, because aerosol processing provided a negative feedback on cloud-droplet number which was not captured if the aerosols were fixed. Interestingly, the opposite phenomena, i.e., increased sensitivity of rainfall to aerosol when processing was permitted, was reported by Miltenberger et al (2018).

In this paper we will use the CASIM microphysics to study the sensitivity of a squall-line of organised-deep convection that occurred over southern China in May 2016. The region receives the majority of its annual rainfall at this time of year, mainly from warm-sector convection. The synoptic situation studied here is one of the most frequently occurring modes of convective organisation in the region (Huang , 2018), hence understanding whether cloud-aerosol interactions can affect the rainfall produced by such systems may have implications for improving predictions of regional rainfall extremes (Luo et al , 2017; Zhang et al , 2018). Moreover, since future generations of operational weather forecast models will be able to include two-way coupling of clouds are aerosols, it is our intention to contribute evidence regarding the role of two-way coupling in short-range predictions of precipitation extremes. Such information will be useful to developers of forecasting systems

when deciding if increasing the complexity of cloud-aerosol coupling is operationally valuable. The impact of aerosol-cloud interactions on model performance will be evaluated by using ground based radar measurements and satellite-remote sensing.

2 Methods

In this section we describe the model experiments and the observations used to evaluate the simulations.

2.1 Model description

This study uses a convection-permitting configuration of the Met Office Unified Model. A description of the model set-up can be found in Furtado et al (2018), together with a detailed description of the non-aerosol components of the CASIM microphysic scheme (see also Grosvenor et al (2017)). In this paper we use the double-moment configuration of CASIM, in which five species of hydrometeor (cloud, rain, ice, snow and graupel) are described by prognostic mass and number concentrations. The aerosol concentrations are either treated as prescribed constants throughout the domain, or are initialised with a spatial homogeneous value that is then allowed to evolve via two-way coupling of the clouds and aerosols. The coupling between the cloud and aerosol fields is described in Miltenberger et al (2018), but the salient features of the coupling are as follows: firstly, aerosols are removed from the air when cloud-droplets are activated (using the parametrization developed by Shipway (2015)); secondly an additional prognostic variable for in-cloud aerosol mass is co-advected with the hydrometeors so that it is transported conservatively through clouds; finally, when cloud particles evaporate, the in-cloud soluble material is returned to the air with a number concentration equal to the number of evaporated hydrometeors. Hence, when aerosols are redeposited during evaporation, their mean size usually exceeds that of the previously activated aerosols (because collision-coalescence gives rain drops that are fewer in number than the cloud droplets from which they develop). This implies that aerosol that were activated as "accumulation"-mode-sized particles can be converted to larger ("coarse") mode particles during evaporation. In section 3 we will compare a simulation with in-cloud processing of aerosol particles to simulations with fixed-number concentrations. A nomenclature for referring to these experiments is established in Table 1. In general, we use the notation N_aF for a fixed-aerosol experiment with number concentration N_a, and refer to the two-way coupled experiment as "1s0dP", where 'P' is for *Processing* and the prefix indicates that there is one species of soluble aerosol particles (1s) no insoluble ("dust") aerosol species (0d). The lack of dust aerosols means that there are no prognostics for aerosol particles that can nucleate ice crystals in the simulation (other than liquid-water droplets). This does not imply that the only pathway to producing ice is homogeneous freezing: heterogeneous freezing is included via a temperature-dependent parametrization for the effects of immersion freezing which specifies the fraction of droplets that become ice nuclei (Cooper , 1986).

2.2 Case overview: 19-21 May 2016 (SR1)

The simulations are evaluated against ground-based radar observations from the Southern China Monsoon Rainfall Experiment (SCMREX; Luo et al (2017)) and satellite-derived estimates of top-of-atmosphere (TOA) radiative fluxes and surface rainfall rates. The case chosen ("SR1") is an example of organised warm-sector convection that occurred between the 19 May and 21

Table 1. Descriptions of the model experiments.

Experiment	description
5$e$$x$F, $x \in \{5, \ldots, 8\}$	fixed-aerosol with number $N_a = 5 \times 10^5, \ldots, 5 \times 10^8$ m^{-3}, and mass $\rho_a = 1.5 \times 10^{-9}$ kg m^{-3}
1s0dP	aerosol-processing with one soluble species intialised with $N_a = 5 \times 10^7$ m^{-3}, $\rho_a = 1.5 \times 10^{-9}$ kg m^{-3}

May 2016 over southern China. A baroclinic environment with a significant amount of large-scale control led to a squall-line of organised deep-convection that propagated along the south coast of China, in Guangdong and Jiangxi provinces. The squall moved eastwards, over a twelve hour period, bringing heavy rain to the coast of Fujian province by 18 UTC 20 May (02 BJT 21 May), before eventually traveling out over the South China Sea.

2.3 Observations and metrics

To evaluated the model simulations we use surface-rainfall retrievals from the Global Precipitation Measurement (GPM) mission, radar observations from the SCMREX campaign and broadband radiant fluxes from the Clouds and the Earth Radiant Eneregy System (CERES) instrument on NASA's *Aqua*. When we compare models and observations, the analysis is conducted after re-griding all the datasets to a fixed latitude-longitude grid with a grid-spacing corresponding to the lowest-resolution data set included in each comparison. A brief description of the observations and some relevant uncertainty estimates are as follows.

2.3.1 GPM

We use post-real-time rainfall estimates from GPM missions' Integrated MultisatelliE Retrievals for GPM (IMERG) dataset. IMERG is a calibrated, multi-sensor retrieval that provides 30-minute, $0.1° \times 0.1°$, estimates of precipitation. The performance of IMERG for east Asia is known to be good in comparison to surface rainfall measurements: Ning et al (2016) reported biases of less than 0.1 mm/day in daily-mean rainfall over 20-month comparison, and showed that IMERG captured both the amount and occurrence frequency of heavy rainfall during that period; Wang et al (2017) investigated cases of extreme rain and showed that IMERG is accurate to within 10 percent over the 20-60 mm/h range.

2.3.2 SCMREX-radar measurements

Measurements of radar reflectivity-factor, Z, are obtained from a S-band radar located in Guangzhou at $(113.35°\text{E}, 23.00°\text{N})$. The maximum range of the radar is approximately 200 km and volume-scans containing 9 elevations are available at intervals of 6 minutes. The azimuthal-resolution of the scans is 1 degree and there are 900 equispaced radial-gates. For comparision to the simulated radar reflectivities, each azimuthal scan is interpolated onto a fixed-height grid as descibed in Furtado et al (2018).
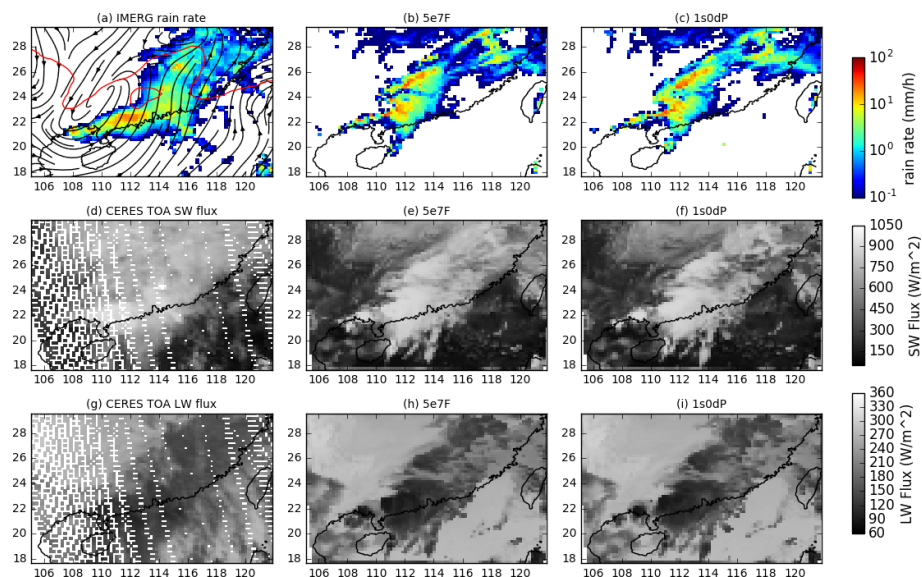
Figure 1. Surface rainfall rates (a-c), outgoing top-of-atmosphere shortwave (d-f) and longwave (g-i) in GPM IMERG (a), CERES-SSF (d,g) and simulations with the 5e7F (b,e,h) and 1s0dP (c,f,i) configurations. The black streamlines and red contour in (a) show the 850 hPa velocity field and the 315 K contour of equivalent potential temperature, respectively, in the ERA Interim reanalysis. The regional coastline is shown in black. All the fields shown are valid within at most 30 minutes of 06 UTC 20 May 2016.

2.3.3 CERES Single-scanner footprint (CERES-SSF)

Top-of-atmosphere longwave (LW) and shortwave (SW) radiative fluxes from the CERES scanning-broadband radiometers are used to provide SW and LW fluxes at 20-km spatial resolution (Wielicki et al , 1996). We use the Aqua edition 3A Single-scanner Footprint (SSF) data which gives calibrated radiances in at 0.3-5 μm, and 8-12 μ with estimated uncertainties of 5 W/m^2 and 2 W/m^2 (Loeb et al , 2007).

3 Results and Discussion

Figure 1 shows observations and simulations at 06 UTC on 19 May (corresponding to a forecast range of 6 hours). The 5e7F (Fig. 1(b,e,h)) and 1s0dP (Fig. 1(c,f,i)) configurations both show a band of rain and cloud extending across the domain from southwest to northeast. Rainfall and outgoing fluxes of longwave and shortwave radiation are qualitatively similar in the two experiments and broadly reproduce the observed structures.

The similarities between the simulated storms disguise large differences in their microphysical structures. The vertical sections in Figure 2 show that inside the squall line 1s0dP has cloud-droplet numbers that are orders of magnitude smaller than those in 5e7F. The number concentrations of other hydrometeors also differ: 1s0dP has greater numbers of rain-drops (colored contours) and lower concentrations of snow particles (grey) than F5e7. Figures 2(c,d) show that these differences are related
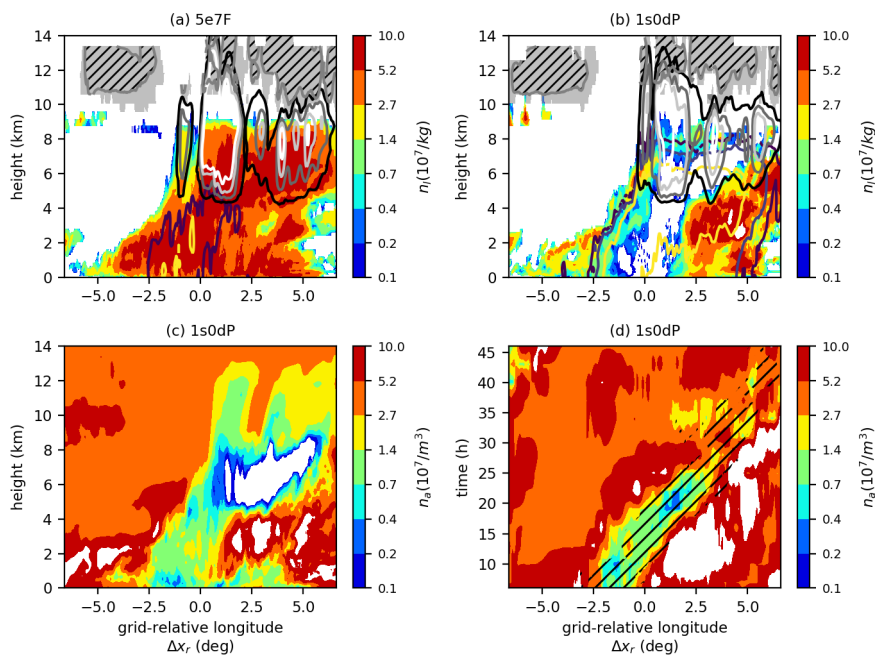
Figure 2. Simulated vertical sections, (a,b,c), and a (rotated-)longitude *versus* time plot, (d) of: hydrometeor number concentrations, (a,b); aerosol number concentration, (c,d). The vertical sections are along a fixed line, $+1.28°$, of rotated-latitude in the rotated-pole coordinate system of the model. The horizontal axes therefore show the grid-relative longitude, Δx_r, relative to the center of the simulation domain in the rotated-pole coordinate system. The vertical coordinate is height in the model's hybrid-height coordinate system. The longitude-time plot is composed of rotated-latitudinal averages at a height of 3405 m in the model's hybrid-height coordinate (approximately 3405 m above the local topographic surface in each grid column). Panel (a) shows the hydrometeor number concentrations for the 5e7F (fixed aerosol) experiment. Panels (b-d) use output from the 1s0dP (aerosol processing) experiment. The colors show the number concentrations of cloud droplets and aerosols, according to the adjacent scales. The colored and grey-scaled contours are lines of constant rain-drop and snow-aggregate number concentration, respectively. In panels (a,b) grey hatched regions indicate where cloud-ice crystals are present. In the longitude-time plot, (d), the hatched region indicates where the surface rain rate exceeds 0.1 mm/h.

to aerosol concentrations inside the squall line, where depletion during activation creates a low-aerosol environment. The longitude-time plot in Figure 2d shows that as the storm propagates a low-aerosol 'core' is maintained, despite the presence of more polluted air outside the squall line. The core region (where most rain falls) therefore has less aerosol and fewer cloud droplets than its surroundings. This "polluted-source – clean-core" structure cannot be replicated in the fixed-concentration simulations: in 5e7F, for example, there is more aerosol inside the squall line and production of rain therefore proceeds in the presence of higher concentrations cloud droplets.

   The responses of cloud and rain to changes in aerosol are shown in Figure 3. The concentrations of cloud droplets in 5e7F are relatively large inside the squall line, compared to 1s0dP, whereas the concentrations of rain droplets are correspondingly
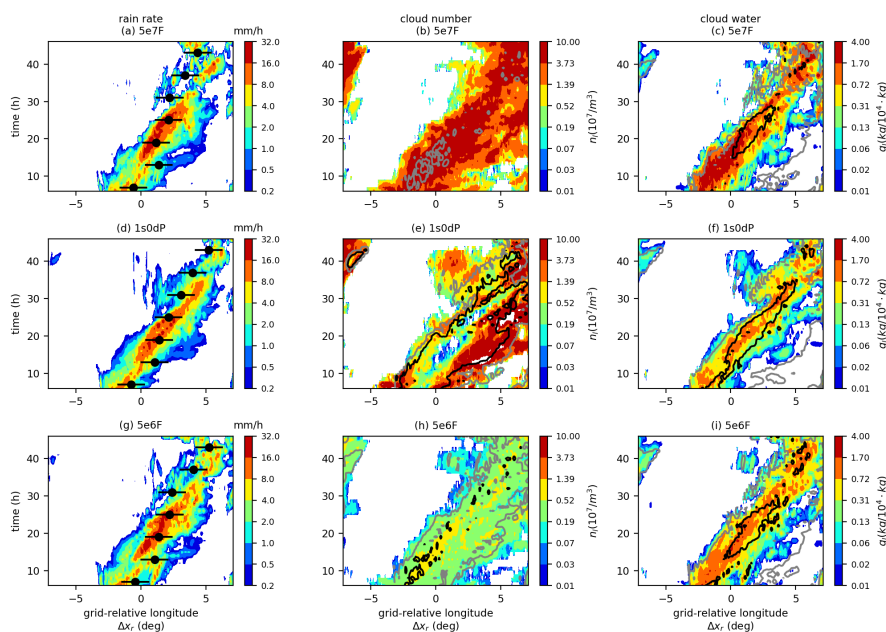
Figure 3. Rotated-longitude–time plots of: surface rainfall rate, (a,d,g); hydrometeor number concentrations, (b,e,h), and mass concentrations, (c,f,i), at a hybrid-height of 3405 m. The horizontal axes show the grid-relative longitude, Δx_r, relative to the center of the simulation domain in the rotated-pole coordinate system. The results from three of the models are shown: 5e7F (a,b,c); 1s0dP (d,e,f); a reduced-aerosol loading experiment, 5e6F, (g,h,i). The colors show rainfall rate or the mass/number concentrations of cloud-liquid droplets, according to the adjacent scales. The solid black and grey contours are lines of constant rain-drop mass or number. The decorated black circles in (a,d,g) show the locations at three-hour intervals of a $2 \times 2°$ box centered on the moving centroid of the surface rainfall-rate field.

smaller. There are analogous differences in the hydrometeor masses: the cloud-liquid water content is largest in 5e7F, and there is a corresponding deficit of rain water. This suggests that the rates of warm-rain processes differ between the experiments. In particular, because 5e7F has more cloud droplets it converts cloud to rain at a slower rate and therefore produces fewer rain drops. Conversely, 1s0dP has faster conversion of droplets which increases rain at the expense of cloud liquid. Despite the

5   differences in composition between the two experiments, the effects on surface rainfall appear to be relatively small (Figs 3(a,d)) There is however a noticeable reduction in the heaviest rainfall rates (greater than 16 mm/h) in 1s0dP which we investigate in more detail below.

By reducing the aerosol-number concentration in a fixed-aerosol experiment, we can assess whether one-way coupling can be 'tuned' to resemble the fully coupled simulation. Figures 3(g-h) show the evolution in a third experiment (F5e6) in which

10   the aerosol has been reduced to a concentration (5×10^6 m^{-3}) that is representative of the squall-line interior in 1s0dP. It can be seen that the reduced-number experiment bears closer resemblance to 1s0dP in terms of hydrometeor concentrations *inside* the squall line but, because it suppresses aerosol numbers throughout the domain, regions outside the squall line have cloud-droplet numbers that are lower than 1s0dP.

8

The mechanisms by which aerosol numbers affect cloud properties can be investigated by considering the evolution of cloud structure in a frame moving with the squall line. To this end, Figure 4 shows the profiles of hydrometeor concentrations averaged over a box around the centroid of surface rainfall. (The path of this box is shown by the black circles in Figs 3(a,d,g) and follows the region of heaviest rainfall.) The two low-aerosol experiments (1s0dP and 5e6F) have fewer cloud-droplets and

5   more rain-drops than 5e7F. Differences in rain-drop numbers (green) are largest close to the melting layer, between 4 and 5 km. The profiles indicate that most rain is produced at these heights, below which the profiles gradually taper towards the surface as drops evaporate. The rain maxima are coincident with peaks in cloud-water content (Figs 4(d-f)), indicating that condensation of liquid cloud is also most active in the 4–5-km layer. The number of cloud-droplets activated in this layer is therefore the dominant factor determining the number of rain drops. By contrast, melting of snow to produce rain imposes an approximate

10   lower bound on rain-drop numbers which is approached as the cloud-droplet number increases.

Moreover, because of the inverse relationship between cloud and rain numbers, the amount of rain is expected to be strongly influenced by the *minimum* cloud-droplet concentrations attained in the cloud. For 1s0dP, aerosol number (Fig. 4; black) decreases with height as droplets form in the ascending air. (Note that above the melting level, the aerosol concentrations in 1s0dP relapse back to larger values, possibly due to entrainment into the ascending air.) Ascending-air parcels eventual achieve

15   lower cloud-droplet numbers than in the fixed-aerosol experiments, which results in a correspondingly larger quantity of rain. The differences in cloud and rain induce variations in frozen clouds between the experiments. For example, there is more graupel in the low-aerosol experiments (because more rain is available for freezing).

The differences in vertical structure between the experiments are consistent with conventional ideas regarding the response of warm-rain processes to aerosol: namely that, *for a given liquid water path*, a 'clean' (low-aerosol) system can achieve a higher

20   surface rainfall rate than a more polluted (high-aerosol) system. This is in contrast to the expected response in regimes that are dominated by melting of frozen precipitation. In the latter case, high cloud-droplet numbers are associated with increased ice-particle production and hence more rainfall. To evaluate whether either of these responses can be detected in the simulation output, Figure 5 shows the relationships between condensed-water paths partitioned according to surface-rainfall rate. It can be seen from Figures 5(a,b) that higher rain water paths are associated with more cloud water and snow aloft. We suggest that

25   figuratively speaking, these association can be considered as representing the internal 'microstructure' of the cloud system. For example, in this case, the structure of convective cores simultaneously results in high condensed water paths and high rainfall rates. Each experiment exhibits a different relationship between cloud- and rain-water path, and therefore generates clouds with different microstructures. The degeneracies in cloud microstructure are due to differences in the aerosol concentrations, particularly within the squall line. For a fixed rate of rainfall (color), lower-aerosol systems attain this rain rate with a less cloud

30   water and more rain water than higher aerosol systems. Alternatively, by considering variations in rainfall along horizontal lines in Figure 5a, we see that a relatively cleaner system can support a higher rainfall rates for a given cloud-water path. This effect can also be illustrated by considering the enhancement in aerosol concentration needed to suppress heavy rainfall by a factor of 1/8, for example, in a convective core with a cloud-water path of, say, 1 kg/m^2: an aerosol loading several orders of magnitudes larger than any considered here would be required.
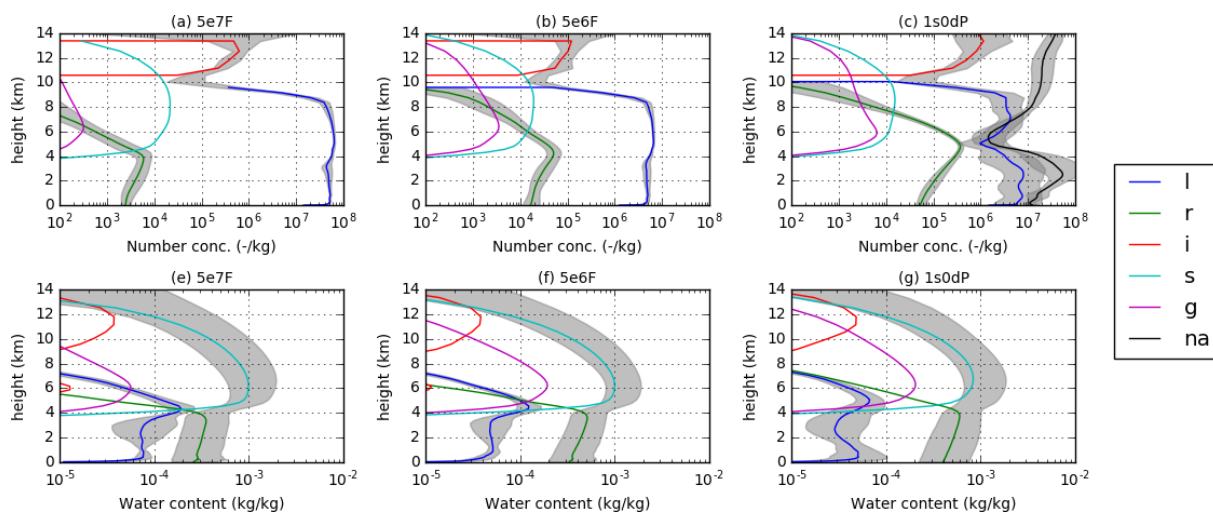
Figure 4. Vertical profiles of hydrometeor number concentrations, (a-c), and mass concentrations, (d-f), time-averaged within a $2 \times 2°$ box moving with the centroid of surface rain rate: (a,d) 5e7F; (b,e) 5e6F; (c,f) 1s0dP. The colors correspond to the hydrometeor species according to the key shown on the left (note that the black line in panel (c) shows the profile of the aerosol number concentration in the aerosol-processing experiment (1s0dP)). The grey regions show the variabilities (defined as ± 1 geometric standard deviation) in the number and mass concentrations of cloud droplets, rain drops and the totality hydrometeor, according to whichever parameter has the largest variability at each point. In panel (c), the standard deviation around the aerosol number concentration profile is also shown.
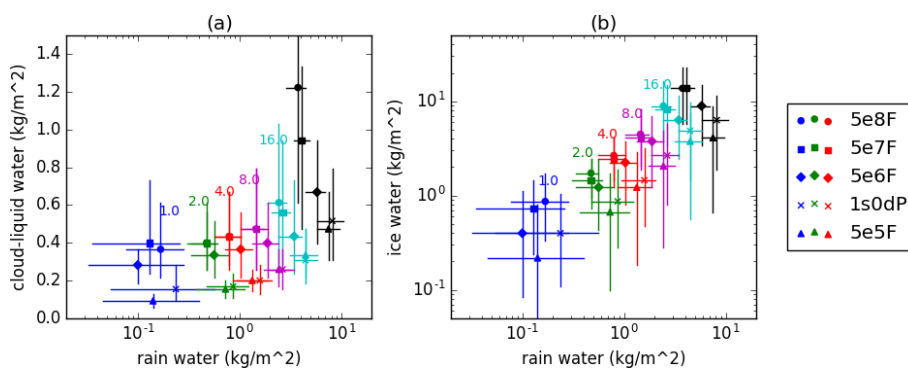

Figure 5. The scaling of (a) cloud-droplet liquid water path, (b) ice water path (snow and ice crystals), with rain water path, partitioned according to surface rainfall rate. The different symbols (circles, squares, etc.) denotes different model experiments, according to the key shown on the right. The colors corresponded to logarithmically spaced surface rainfall intervals, the upper bound of each interval is indicated by the colored text on the plots (e.g, the red-colored points correspond to grid points where the rain rate was between 2 and 4 mm/h). The horizontal and vertical bars show the inter-quartile ranges in each interval for the ordinate and coordinate variables.

The relationships between cloud- and rain-water paths shown in Figure 5a support the conclusion that (for this case) aerosol concentration affects the simulated clouds by modifying the rate at which liquid cloud converts to rain drops. By contrast,

cold-cloud processes seem to be largely passive because the variations in ice-water path and graupel can be understood as a response to the rain-water changes: increased rain water leads to more graupel via heterogeneous freezing; similarly, decreased cloud water leads to less water being available for nucleating ice and snow crystals.

The preceding discussion demonstrates that the treatment of aerosols affects the microphysical structure of the squall line.
5 However, the preliminary inspection of rainfall and long-wave fluxes in Figures 1 and 3 suggest that the hydrological and radiative impacts of these changes are not large (compared to forecast errors that are common to all the simulations). We now present a more detailed analysis of rainfall and top-of-atmosphere radiation which reveals that systematic differences do exist between the simulations. Figure 6 shows histograms of radar reflectivity, surface-rainfall rate and TOA SW-flux. The simulated histograms of reflectivity are increasingly shifted towards smaller values of dBZ as aerosol number decreases. The effects of
10 these shifts are particularly pronounced in the large-dBZ tails of the distributions, where the cleaner experiments (1s0dP and 5e6F) have lower frequencies. This shift is related to a corresponding skewing of the rainfall-rate histograms towards lighter rain in the cleaner simulations. Reflectivity factor and rainfall flux are determined by moments of the drop-size distribution, hence their ratio contains information about the typical radii of the drops present. If the reflectivity is conditionally sampled based on the surface-rainfall rate, we can interpret the variability of reflectivity with aerosol number in each rainfall interval
15 as being due to variability in the typical-drop size. The colored circles in Fig. 6b show the mean reflectivity in three rain-rate intervals. Because the clean-experiment histograms are skewed toward lower values of dBZ, the mean reflectivity in each rain-rate intervals decreases with decreasing aerosol number. This is consistent with lower cloud-droplet numbers giving rise to more numerous but smaller rain drops, because conversion of droplets to rain proceeds more rapidly.

The relationship between independent measurements of surface-rain rate and reflectivity is a directly observable way of
20 quantifying the microphysical structure of the squall line. Moreover, in the simulations this relationship is strongly modulated by aerosol concentration. The simulated "(dB)Z-R" relationships (colored circles in Fig. 6b) can be compared to the relationship derived from the radar and IMERG measurements (black circles). Interestingly, despite biases in the underlying histograms of rainfall and reflectivity, the measurement-derived relationship is spanned by the simulations. These relations are structural properties that emerge from representations of microphysical processes in the models. Therefore, although the
25 simulated relationships may result from compensating biases[2], they still assess how well the models perform at capturing the observed co-variability of precipitation properties.

Measurements of top-of-atmosphere radiation can also be used to evaluate the performance of the simulations. Figure 6c evaluates histograms of outgoing-SW flux against the CERES-SSF measurements. The simulated distributions overestimate the frequency of occurrence of points with low reflected-solar flux (100–300 W m^{-2}) and underestimate the occurrence of fluxes greater than 600 W m^{-2}).
30 The models show better agreement with the observations for fluxes that are intermediate between these two extremes (300–600 W m^{-2}). To understand which types of cloud cause the model biases in different parts of the histograms, the colored markers in Fig. 6c show the water paths of rain (squares) and cloud-liquid (circles), averaged over the three SW-flux intervals. The overestimated, low-flux peaks are associated with the presence of lightly or non-precipitating

---

[2]In this respect, if it interesting to note that the model with the best rain-rate histogram (5e5F) has the largest discrepancy from the observed Z-R relationship.
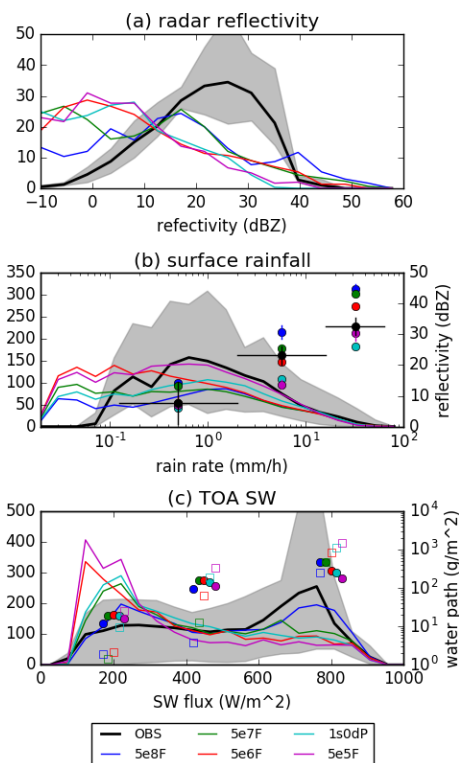
Figure 6. Time-mean histograms (solid lines) of: (a) radar reflectivity, (b) surface rainfall rate, (c) outgoing SW-flux, in the model experiments compared to the observations. The grey shaded area shows the range (from minimum to maximum number of counts) for the observations, in each variable-bin. In panel (b) the colored circles show the mean radar reflectivity in three surface-rainfall intervals for the simulations (colors) and IMERG retrievals (black). The horizontal bars on the IMERG-points show the lengths of each intervals. In panel (c) the colored symbols show the mean cloud-water paths (circles) and rain-water paths (squares) in three contiguous SW-flux intervals, for the simulations.

clouds with low ratios of rain-to-cloud, whereas the underestimated fluxes are in an interval that is dominated by columns with high liquid water paths. The high liquid-water content regions are due to the passage of the squall line across the domain. This suggests that the overestimates at low-fluxes are due to insufficient stratiform cloud cover in the regions away from the deep-frontal clouds. This error is least in the most polluted experiment (5e8F), which is consistent with the suppressed autoconversion in the experiment causing an increase in the prevalence or longevity of liquid water clouds in that simulation. From the short-wave flux histograms, it is evident that 5e8F redistributes the low-rain-water content pixels into brighter parts of the SW distribution, where they coincide in terms of reflected flux with the deep-frontal clouds. Conversely, the underestimates of shallow-cloud amount are largest for the cleanest of the fixed-number experiments, because rapid conversion of cloud to rain reduces the amount of liquid cloud these simulations can produce.

To investigate further the cloud changes that are responsible for the differences in TOA radiation between the experiments, Fig. 7 shows the total condensed water path in each of three SW-flux intervals for the MODIS/CERES observations and a subset
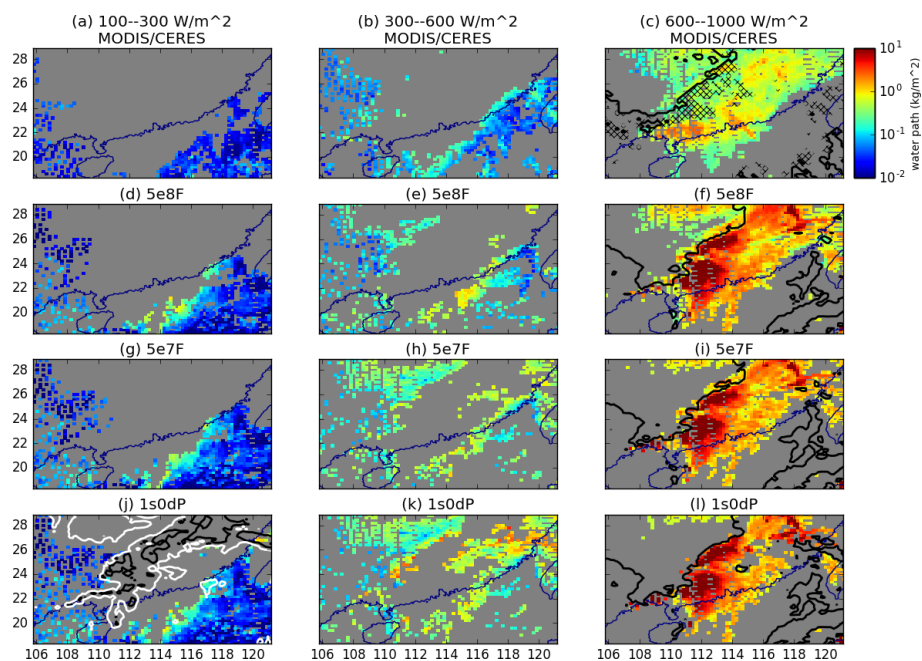
Figure 7. Total condensed water path (all species of hydrometeor) in the MODIS observations (a-c), 5e8F (d-f), 5e7F (g-i) and 1s0dP (j-l). The fields are partitioned into three SW-flux intervals: fluxes between 100 and 300 W m^{-2} (a,d,g,j); fluxes between 300 and 600 W m^{-2} (b,d,h,k); fluxes greater than 600 W m^2 (c,f,i,l). For each panel, points outside the corresponding interval of fluxes have been masked out in grey. The black contour in (c,f,i,l) encloses the regions where the fraction (by mass) of the total condensed water path that is ice exceeds 20 percent. In panel (j) the contours show where the column integrated aerosol in the lowest 5 km of the atmosphere are 20 percent (black) and 80 percent (white) of the domain-mean aerosol path.

of the simulations. The fields are compared for a single overpass time of the satellite. For each SW-flux interval, grid-points with radiances outside that interval have been masked. The most polluted simulation, 5e8F, produces the most realistic field of clouds. In particular, it is the only configuration that is able to produce a region of realistically bright stratus in the wake of the squall line (in the north-west corner of the domain). Stratus clouds also exists in the other simulations (eg, Figs 7(e,h,k)), but are less bright than in the retrievals.

5   The regions with deep ice clouds (which for the models can be defined as where the ice water path exceeds 20 percent of the total water path[3]) are shown by the black lines in Figs 7(c,f,i,l) As the aerosol-number concentration decreases, the number of grid-points with ice cloud which have radiances greater than 600 W/m^2 decreases (Figs 7(f,i,l)). The SW-fluxes reflected from these points fall instead into the low-radiance intervals, which are overpopulated with pixels compared to the

10   MODIS/CERES estimates. Figures 7(j-l) show the results from the processing experiment, 1s0dP. The water paths in this experiment are intermediate between the fixed-number experiments: behind the squall line, it resembles the cleaner fixed-number experiment (5e7F); within the squall, it has fewer high-condensed-water path (higher brightness) columns than 5e7F.

---

[3]For the MODIS retrievals we can demarcate an ice region as those pixels for which MODIS retrieves either mixed-phase of ice cloud (Fig. 7c).

Atmospheric
Chemistry
and Physics
Discussions

Open Access

EGU

The differences between the rainfall frequency distributions shown in figure 6b suggest that there may be detectable effects of aerosols on the mean properties of surface rainfall during this case. Since it such averages, rather than the statistical distribution of rainfall which are of primary importance of regional-scale hydrology we conclude this section by examining the time series of average rainfall characteristics in Figure 8. To characterise rainfall, we adopt the commonly used approach of decomposing

5 the hourly instantaneous surface-rainfall rates into contributions from the areal coverage of rainfall (rainfall frequency) and the mean intensity of rainfall at rainy points (rainfall intensity). These quantities are defined relative to a threshold minimum rain rate of 0.1 mm/h (chosen to reflect the lower limit of the IMERG retrievals). Hence, if A is the total area of the domain, then the frequency, f, is given by $f = \sum^> \Delta_{\mathbf{x}}/A$, where the summation is over points $\mathbf{x}$ where rainfall exceeds the threshold, and $\Delta_{\mathbf{x}}$ is grid-box area. Similar, the intensity $I = \sum^> p_{\mathbf{x}}\Delta_{\mathbf{x}}/Af$, where p is the surface-rainfall rate, and amount $P = I \times f$.

10 Figure 8a shows that rainfall intensities (solid lines) increase with increasing aerosol concentration. The most polluted simulations have surface rainfall that is up to 50 percent more intense than the least polluted experiments. The aerosol-processing experiment has intensities that are intermediate between the least-polluted and most-polluted experiments. This is consistent with the observation made above that for lower rain rates the histogram of rain rates for 1s0dP is similar to the higher-fixed-number experiments (5e7F and 5e8F) whereas for higher rain rates it is similar to the least polluted scheme (5e5F).

15 The sizes of the circles in Fig. 8 show the relative differences in the frequency of rainfall for each simulation. It can be seen that the cleaner experiments have rainfall over a larger fraction of domain, which is consistent with the rainfall (and reflectivity) histograms becoming progressively more shifted towards lower rain rates (and reflectivity factors) as the aerosol number concentration decreases. The overall dependence of surface rainfall on aerosol can therefore be characterised as a transition towards a regime of more-frequent, less-intense rainfall as the aerosol number increases. By capturing both high- and

20 low-aerosol concentrations in the same domain, the aerosol-processing experiment is able to combine aspects of both the low- and high-intensity regimes and therefore gives surface rainfall properties that are intermediate between the clean and polluted extremes. The opposing tendencies in f and I are consistent with Miltenberger et al (2018) who found that convective-cell size increased (indicating more intense rainfall) whereas the number of cells decreased with increasing amounts of aerosols (indicating a smaller in the rainy area). Finally, in Fig. 8b, we see that the amount of surface rainfall is *marginally* higher

25 in cleaner simulations, because (for this case) rainfall amount is slightly dominated by the rain-frequency differences, offset by an opposing tendency due to the decrease in intensity with aerosol number. It should also be noted that, because of the opposing influences of aerosols on f and I the difference in rainfall amount between the least- and most-polluted simulations are relatively small (of the order of at most 20 percent).

4 Conclusions

30 We have investigated how the representation of cloud-aerosol interactions influence simulations of a heavy-rainfall event over south China. Experiments with fixed-aerosol numbers, which spanned a range of ambient-air conditions (from relatively polluted to extremely clean), were used to demonstrate the effects of aerosols in one- and two-way coupled modeling frameworks. In the one-way coupled experiments the aerosol populations are not modified by cloud processes. In the two-way coupled
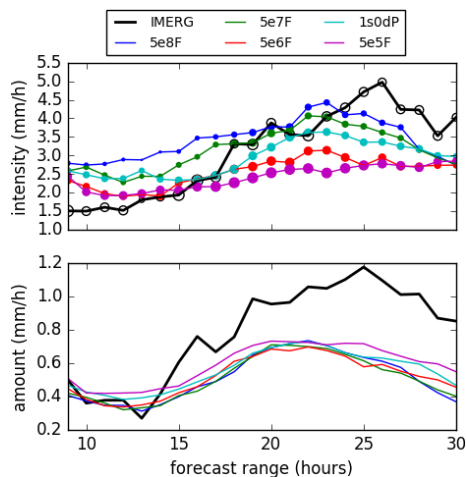
Figure 8. Time series of (a) domain averaged rainfall intensity (lines) and frequency (circles), (b) rainfall amount, in the models (colors) and IMERG retrievals (black). The time is given in hours elapsed since the initialisation of the forecasts (00 UTC 20 May).

model, the interstitial aerosols are depleted by activation of droplets and re-populated when hydrometeors evaporate. Satellite retrievals and ground-based radar measurements have been used to place the inter-model spread (and hence uncertainties in cloud-aerosol effects) into the context of measurable properties of the evolving system of clouds.

We have shown that, for the simulations performed here, the dominant mechanism by which areosols influence clouds and precipitation is a 'warm-rain' pathway, whereby reducing aerosols decreases the timescale for producing rain and increases rain water at the expense of cloud droplets. This effect is particularly evident if the water paths of cloud and rain are compared at approximately constant values of the rainfall rate (because cloud-water path and rain-water path vary inversely to each other in a given rain-rate interval). Conversely, the same analysis shows that the lower the aerosol loading, the greater the rainfall that can result for a fixed cloud-water path. For the regime (organised warm-sector convection, with large-scale forcing) and model considered, melting of ice crystals provides a lower bound on achievable rain-drop numbers.

Reductions in the mass of water suspended as cloud-droplets are accompanied by decreases in the brightness of the simulated clouds, particularly in regions away from any deep ice-clouds. Aerosols also alter the properties of rainfall reaching the surface: in the more polluted simulations, the rainfall is more intense (with higher rainfall rates when rain occurs) but occurs over a smaller spatial area. As a consequence of these competing changes, the amount of rainfall reaching the surface (the domain mean) is relatively insensitive to aerosol concentration. This latter point may have been anticipated because on the timescales of individual weather events the amount of rainfall is strongly constrained by large-scale convergence into the rainy regions at low levels.

The changes in rainfall intensity and rain fraction are manifestations of underlying changes in the probability distributions of surface rainfall. We have shown that simulations with fewer aerosols have more frequent lower rain rates than polluted

experiments. A corresponding reduction in the occurrence of high values of radar reflectivity factor with decreasing aerosol number was detected when the simulated radar reflectivity factors were compared to measurements

The inclusion of two-way coupling between aerosols and clouds was shown to qualitatively change the simulations, in a manner that can not be replicated in a fixed-number experiment. In terms of the quantities assessed, the processing experiment

5 is intermediate between a relatively polluted fixed-aerosol experiment (with the same initial aerosol concentration) and a much cleaner simulation with a lower number concentration. This happens because activation removes aerosols from the ambient air, so the presence of deep-convection maintains a low-aerosol 'core', within which most the heavy rain forms. Rainfall is therefore produced mainly from cloud droplets which are less numerous than would be the case if the aerosol number was unaffected by activation. The result is that in a two-way coupled experiment the 'warm-rain' pathway to more vigorous then it would be

10 in fixed-aerosol number experiment with the same initial conditions. The aerosol processing experiment therefore resembles a 'cleaner' fixed-number simulation in terms of the partitioning of water between cloud and rain inside the squall line. Outside the squall line, the opposite situation prevails: the aerosol population recovers towards the environmental value so any shallow clouds are in relatively polluted environments compared to squall line's interior. Hence, stratiform precipitation is produced from clouds with high cloud droplet numbers. The ability to represent different cloud-droplet numbers in different parts of the

15 domain (in a way that depends on precursory cloud processes) may well be the main advantage of aerosol-processing models. Here we have shown that capturing these dependencies can be important for simulating organised convection and affects both the hydrological and radiative impacts of such systems, in a manner consistent with –but not fully replicable by– one-way coupled simulations with tunned aerosol concentrations.

Two aspects not addressed in this paper may form the basis fore future work: firstly, our analysis has been limited to a single

20 case; secondly, we have omitted any discussion of ice-nucleating aerosols. Although single cases are useful for identifying mechanisms, they need to be supplemented by extended trails to quantify the affects on model performance. As part of such trails, it will be necessary to use observed (or at least re-analysed) aerosol concentrations to drive the models with realistic cloud nuclei. Moreover, in this paper, we have not considered the effects of ice-nucleation parameterizations –we plan to address this in the future as part of forecast trails with a range of microphysical configurations.

25 *Code and data availability.* The CERES/Aqua Level 2 Single-Scanner Footprint Edition 3A observed TOA Fluxes can be obtained from the Atmospheric Sciences Data Center at NASA Langley Research Center: https://ceres-tool.larc.nasa.gov/ord-tool. The MODIS/Aqua Collection 6 Level 2 Cloud Product data can be obtained from the Level-1 and Atmosphere Archive and Distribution System Distributed Active Archive Center in the Goddard Space Flight Center: https://ladsweb.modaps.eosdis.nasa.gov/archive. The reflectivity measurements from the Guangzhuo radar and the postprocessed model data can be obtained from the SCMREX data archive: http://exps.camscma.cn/scmrex The

30 Integrated MultisatellitE Retrievals for GPM (IMERG) can be obtained from NASA's Precipitation Processing Center: ftp://arthurhou.pps.eosdis.nasa.gov//gpmdata. The Python code used is available for download from https://code.metoffice.gov.uk/trac/home.

Author contributions. KF conducted the model experiments and analysed the results. YL and TJ conceived and instigated the work. YL provided SCMREX data from the Guangzhou Radar. PF provided scientific oversight throughout. AH and others developed the microphysics scheme code. All authors worked on the manuscript text.

Competing interests. None known.

References

Albrecht, B. A.: Aerosols, cloud microphysics, and fractional cloudiness, Science, 245, 1227-1230, https://doi.org/10.1126/science.245.4923.1227, 1989.

Cooper, W. A.: Ice Initiation in Natural Clouds. In: Precipitation Enhancement–A Scientific Challenge. Meteorological Monographs. American Meteorological Society, Boston, MA. 1986.

Fan, J., Leung, L. R., Li, Z., Morrison, H., Chen, H., Zhou, Y., Qian, Y., and Wang Y.: Aerosol impacts on clouds and precipitation in eastern China: Results from bin and bulk microphysics, J. Geophys. Res., 117, D00K36, doi:10.1029/2011JD016537. 2012.

Feingold, G., and Kreidenweis, S. M.: Cloud processing of aerosol as modeled by a large eddy simulation with coupled microphysics and aqueous chemistry, J. Geophys. Res., 107(D23), 4687, doi:10.1029/2002JD002054, 2002.

Furtado, K., Field, P. R., Luo, Y., Liu, X., Guo, Z., Zhou, T., et al. Cloud microphysical factors affecting simulations of deep convection during the presummer rainy season in Southern China. Journal of Geophysical Research: Atmospheres, 123, 10,477-10,505. https://doi.org/10.1029/2017JD028192, 2018.

Grosvenor, D. P., Field, P. R., Hill, A. A., and Shipway, B. J.: The relative importance of macrophysical and cloud albedo changes for aerosol-induced radiative effects in closed-cell stratocumulus: Insight from the modelling of a case study. Atmospheric Chemistry and Physics, 17, 5155-5183. https://doi.org/10.5194/acp-17-5155-2017, 2017

Hill, A. A., Shipway, B. J., and Boutle, I. A.: How sensitive are aerosol-precipitation interactions to the warm rain representation?, J. Adv. Model. Earth Syst., 7, 987-1004, https://doi.org/10.1002/2014ms000422, 2015.

Huang, L., Luo, Y., and Zhang, D.-L.: The relationship between anomalous Presummer extreme rainfall over south China and synoptic disturbances. Journal of Geophysical Research: Atmospheres, 123, 3395-3413. https://doi.org/10.1002/2017JD028106, 2018.

Johnson, J. S., Cui, Z., Lee, L. A., Gosling, J. P., Blyth, A. M., and Carslaw, K. S.: Evaluating uncertainty in convective cloud microphysics using statistical emulation, J. Adv. Model. Earth Syst., 7, 162-187, https://doi.org/10.1002/2014MS000383, 2015.

Kaufman, Y. J., Koren, I., Remer, L. A., Rosenfeld, D., and Rudich, Y.: The effect of smoke, dust, and pollution aerosol on shallow cloud development over the Atlantic Ocean, Proc. Natl. Acad. Sci. U. S. A., 102, 11,207-11,212, doi:10.1073/pnas.0505191102. 2005.

Khain, A. P., BenMoshe, N., and Pokrovsky, A.: Factors Determining the Impact of Aerosols on Surface Precipitation from Clouds: An Attempt at Classification. J. Atmos. Sci., 65, 1721-1748, https://doi.org/10.1175/2007JAS2515.1. 2008

Loeb, N. G., Kato, S., Loukachine, K., and Manalo-Smith, N.: Angular distribution models for top-of-atmosphere radiative flux estimation from the clouds and the earth's radiant energy system instrument on the Terra Satellite. Part I: Methodology. Journal of Atmospheric and Oceanic Technology, 22, 338-351, 2007

Luo, Y., Zhang, R., Wan, Q., Wang, B., Wong, W. K., Hu, Z., Jou, B. J., Lin, Y., Johnson, R. H., Chang, C., Zhu, Y., Zhang, X., Wang, H., Xia, R., Ma, J., Zhang, D., Gao, M., Zhang, Y., Liu, X., Chen, Y., Huang, H., Bao, X., Ruan, Z., Cui, Z., Meng, Z., Sun, J., Wu, M., Wang, H., Peng, X., Qian, W., Zhao, K., and Xiao. Y. (2018). The Southern China Monsoon Rainfall Experiment (SCMREX) Data Archive, http://exps.camscma.cn/scmrex/management/main!main.action.

Miltenberger, A. K., Field, P. R., Hill, A. A., Rosenberg, P., Shipway, B. J., Wilkinson, J. M., Scovell, R., and Blyth, A. M.: Aerosol-cloud interactions in mixed-phase convective clouds - Part 1: Aerosol perturbations, Atmos. Chem. Phys., 18, 3119-3145, https://doi.org/10.5194/acp-18-3119-2018, 2018.

Ning, S., Wang, J. and Jin, J. and Ishidaira, H.: Water 2016, 8(11), 481; https://doi.org/10.3390/w8110481, 2016.

Rosenfeld, D., Lohmann, U., Raga, G. B., O'Dowd, C. D., Kulmala, M., Fuzzi, S., Reissell, A., and Andreae, M. O.: Flood or drought: How do aerosols affect precipitation?, Science, 321, 1309-1313, https://doi.org/10.1126/science.1160606, 2008.

Shipway, B. J.: Revisiting Twomey's approximation for peak supersaturation, Atmos. Chem. Phys., 15, 3803-3814, https://doi.org/10.5194/acp-15-3803-2015, 2015.

5 Tao, W.-K., Chen, J.-P., Li, Z., Wang, C., and Zhang, C.: Impact of aerosols on convective clouds and precipitation, Rev. Geophys., 50, RG2001, https://doi.org/10.1029/2011RG000369, 2012.

Twomey, S.: The influence of pollution on the shortwave albedo of clouds, J. Atmos. Sci., 34, 1149-1152, https://doi.org/10.1175/1520-0469(1977)034<1149:TIOPOT>2.0.CO;2, 1977.

Wang, R., Chen, J., and Wang, X. (2017). Comparison of IMERG Level-3 and TMPA 3B42V7 in Estimating Typhoon-Related Heavy Rain.

10 Wielicki, B. A., Barkstrom, B. R., Harrison, E. F., Lee, R. B., Smith, G. L., and Cooper, J. E.: Clouds and the Earth's Radiant Energy System (CERES): An Earth observing system experiment. Bulletin of the American Meteorological Society, 77, 853-868, 1996.

Zhang, X.: Application of a convection-permitting ensemble prediction system to quantitative precipitation forecasts over southern China: Preliminary results during SCMREX, Q J R Meteorol Soc 144:2842-2862. https://doi.org/10.1002/qj.3411, 2018